Journal of Solid State Chemistry **164,** 106–109 (2002)
doi:10.1006/jssc.2001.9453, available online at http://www.idealibrary.com on IDEAL®

The Synthesis of SnS_2 Nanoflakes from Tetrabutyltin Precursor

Qing Yang,* Kaibin Tang,*,[1] Cunrui Wang,* Daoyuan Zhang,† and Yitai Qian*,[1]

*Department of Chemistry and Structure Research Laboratory, University of Science and Technology of China, Hefei, Anhui 230026, People's Republic of China; and †Astronomy and Applied Physics, University of Science and Technology of China, Hefei, Anhui 230026, People's Republic of China

Received August 29, 2001; in revised form October 25, 2001; accepted November 12, 2001

Hexagonal phase SnS_2 nanoflakes have been synthesized by reactions between an organotin precursor tetrabutyltin [TBT, $(CH_2CH_2CH_2CH_3)_4Sn$] and carbon disulfide in hexanes at 180–200°C for 10-40 h. The structure, morphologies, composition, and properties have been characterized by powder X-ray diffraction (XRD), transmission electron microscopy (TEM), selected area electron diffraction (SAED), X-ray photoelectron spectroscopy (XPS), ICP-AES, and Raman and Mössbauer spectroscopies. XRD patterns determined the hexagonal SnS_2 with lattice parameters $a = 3.6384$ Å, $c = 5.9201$ Å obtained in *n*-hexane, and $a = 3.6389$ Å, $c = 5.9288$ Å in cyclohexane. The flakelike morphologies were mainly caused by the anisotropic growth of SnS_2. A possible mechanism is given in the paper.

Key Words: **chalcogenide; SnS_2; semiconductors; tetrabutyltin; precursor; solvothermal crystal growth**

1. INTRODUCTION

In the past few decades, metal chalcogenides have been extensively studied because of their potential application in electronic, optical, and superconductor devices (1–3). Tin sulfides, as the IV–VI intermetallic compounds, possess many semiconducting properties. SnS_2 belongs to the interesting class of isomorphic materials that are in many ways between two-dimensional (layer type) systems and three-dimensional crystals, and it exhibits a strong anisotropy of optical properties (4). SnS_2 is a layered semiconductor with a band gap of about 2.35 eV (5) and therefore should have the potential to work as an efficient solar cell material (6). It is also of interest in holographic recording systems and electrical switching (7, 8).

Various methods have been employed for the preparation of SnS_2. For example, single crystals of SnS_2 have been grown by chemical vapor transport (CVT) and physical vapor transport (PVT) (9–11). Bulk SnS_2 has been synthesized through direct reaction of the elements (12, 13), solid state reactions (14, 15), mechanochemistry (16), and pyrolysis of organotin precursors [$(R_2SnS)_3$ or $(R_3Sn)_2S$; $R = Ph$, $PhCH_2$] (17, 18). Thin films of SnS_2 have been synthesized through CVT (19), PVT (20), the Bridgman–Stockbager technique (21), molecular beam epitaxy (MBE) (22), spray pyrolysis (23), successive ionic layer adsorption and reaction (SILAR) (24), and different kinds of chemical vapor deposition (CVD) (25–28). Meanwhile, the solvothermal method, as a useful synthetic route, has been employed for the production of SnS_2 ultrafine crystallites from the inorganotin Sn source in our previous studies (29). However, to date, the preparation of SnS_2 from an organotin precursor through the solvothermal synthetic route has not been reported. In this paper we focus on the use of tetrabutyltin [TBT, $(CH_2CH_2CH_2CH_3)_4Sn$], an organotin precursor, as the first study of the synthesis of SnS_2 nanocrystallites through the solvothermal route.

2. EXPERIMENTAL

Reagents. The chemically pure reagents TBT, CS_2, solvents (*n*-hexane and cyclohexane), and deionized water were used in the experiments. TBT was purchased from Merck-Schuchardt Corp. of Germany. CS_2 was obtained from Shanghai Chemical Reagent Ltd. Corp. of China. Others were purchased from different chemical reagent corporations.

Procedure. In a typical procedure for the preparation of SnS_2, nanocrystallites were obtained from the solvothermal reactions between TBT and CS_2 in hexanes. First, 1 ml of TBT and 2–3 ml of CS_2 were dissolved in 20 ml of *n*-hexane, respectively. Thereafter, the two solutions were put into a Teflon-lined stainless steel autoclave of 50-ml capacity in sequence. The autoclave was then sealed and maintained at 180–200°C for 10–40 h, and cooled to room temperature naturally. The final precipitates were obtained and washed with CS_2, hexane, and deionized water to remove the by-product of elemental sulfur and other impurities and then

[1] To whom correspondence should be addressed. K. Tang: Fax; +86-551-3601600; E-mail: kbtang@ustc.edu.cn.

0022-4596/02 $35.00

dried in a vacuum at 60°C for 3 h. Other experiments with cyclohexane replaceing *n*-hexane and with different feedstock were also carried out.

Characterization. Powder X-ray powder diffraction (XRD) was carried out on a China Dandong X-ray diffractometer with graphite-monochromatized Cu $K\alpha_1$ radiation ($\lambda = 1.54178$ Å). The scanning rate of 0.06°/s was applied to record the patterns in the 2θ range of 10° to 70°. The reflection data were collected at ~ 25°C. The morphology and the size of the products were observed by transmission electron microscopy (TEM), carried out on a Hitachi H-800 transmission electron microscope. Meanwhile, electron diffraction (ED) was also conducted. Samples were prepared by placing a drop of dilute alcohol suspension of SnS_2 nanocrystallites dispersed by using a supersonic disperser onto an amorphous carbon-coated copper grid and then wicking away the solution. The electronic binding energy of the samples was examined by X-ray photoelectron spectroscopy (XPS), which was recorded on a VGESCALAB MKII X-ray photoelectron spectrometer using non-monochromatized Mg $K\alpha$ ($h\nu = 1253.6$ eV) X ray as the excitation source with an energy resolution of 1.0 eV. Binding energies were calibrated to the internal standard C 1*s* peak (284.6 eV). Element analysis was done by ICP-AES, which was carried out on an Atomscan Advantage (Thermo Jarrell Ash Corp.). The Raman spectrum was recorded on a Spex 1403 Raman spectrometer ($\lambda = 514.5$ nm) at ambient temperature. The spectra of the samples were obtained in the range 100 to 600 cm^{-1} at a laser power of 150 mW with a slit of 140 μm (~ 1 cm^{-1}) and an integration time of 0.5 s per step. ^{119}Sn Mössbauer spectroscopy was recorded at room temperature in the constant-acceleration mode on an Oxford MS-500 Mössbauer spectrometer with a $Ba^{119m}SnO_3$ ã-ray source. The velocity scale was calibrated with the magnetic sextet spectrum of a high-purity iron foil absorber with a ^{57}Co(Rh) source.

3. RESULTS AND DISCUSSION

Structure identification of the as-prepared samples was carried out using the XRD patterns, shown in Fig. 1. The patterns (Fig. 1a) show that the as-prepared samples (in *n*-hexane) are the hexagonal SnS_2 phase with lattice parameters $a = 3.6384$ Å, $c = 5.9201$ Å, in accord with the reported data (JCPDS Card File, 23-677, $a = 3.6486$ Å, $c = 5.8992$ Å). Figure 1b also shows that the obtained SnS_2 in cyclohexane is the hexagonal phase, with lattice parameters $a = 3.6389$ Å, $c = 5.9288$ Å. By means of XRD analysis, no impurities are detected.

Figure 2a shows that the SnS_2 crystallites (in *n*-hexane) have flakelike morphologies. Figure 2b is the image of a complete hexagonal flake obtained in the route. The corresponding ED patterns (Fig. 2c) show that the flake has

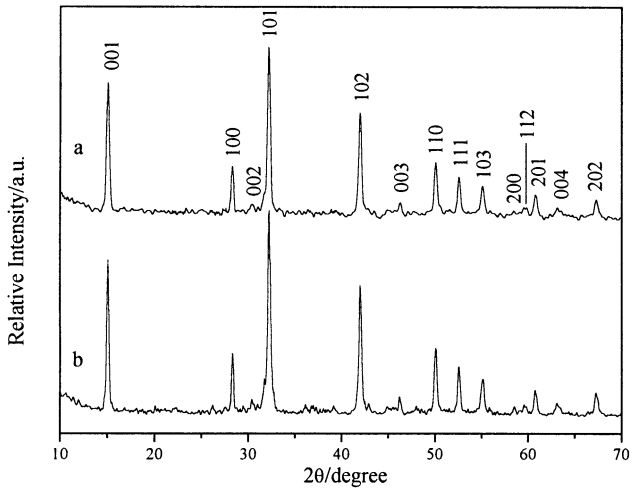

FIG. 1. Powder XRD patterns of the samples (a) obtained in *n*-hexane and (b) in cyclohexane.

single-crystal nature. Figure 2d demonstrates that the crystallization of the sample obtained in the route for 10 h is not as good as that for 40 h (shown in Figs. 2a and 2b). The SnS_2 crystallites obtained in cyclohexane had similar morphologies (not shown).

XPS has been used to investigate the samples prepared in the route. The survey XPS of the samples reveal two strong peaks indicating the existence of Sn and S. Very little contaminated oxygen was absorbed in the samples. The close-up spectra of the samples are used to determine the oxidation states of elements. The obtained value of the bonding energies for Sn $3d_{5/2}$ is 486.60 eV in *n*-hexane and 486.65 eV in cyclohexane, which are near the reported value for Sn^{IV} in SnS_2 (30). Although the value is near that in SnO_2 (31), SnO_2 could not be produced in the route because of the oxygen-free reaction system. The Sn close-up spectra also imply no SnS (Sn $3d_{5/2}$, 485.60 eV) (30a,32) has been produced. The S 2*p* binding energies of the SnS_2 nanocrystallites are 161.55 eV in *n*-hexane and 161.65 eV in cyclohexane, respectively. The results demonstrate that no elemental sulfur (164.05 eV) (30b) is contained in the product. Quantification of the as-prepared SnS_2 has been given by a direct elemental analysis of ICP-AES and it gives the molar ratio of Sn:S as 1.000:2.046 in *n*-hexane and 1.000:2.032 in cyclohexane, respectively. The results reveal that the obtained crystallites are stoichiometric.

The Raman spectra of the as-prepared SnS_2 nanoflakes are shown in Fig. 3, which exhibit an intense peak at about 311 cm^{-1}, corresponding to A_{1g} mode according to the group theory analysis given by Lucovsky *et al.* (33). In the route, the peak located at about 210 cm^{-1} of the first-order E_g mode has not been obviously observed. The disappeared peak of the E_g mode probably results from the nanosize effect according to Abello *et al.*'s analysis (34). The

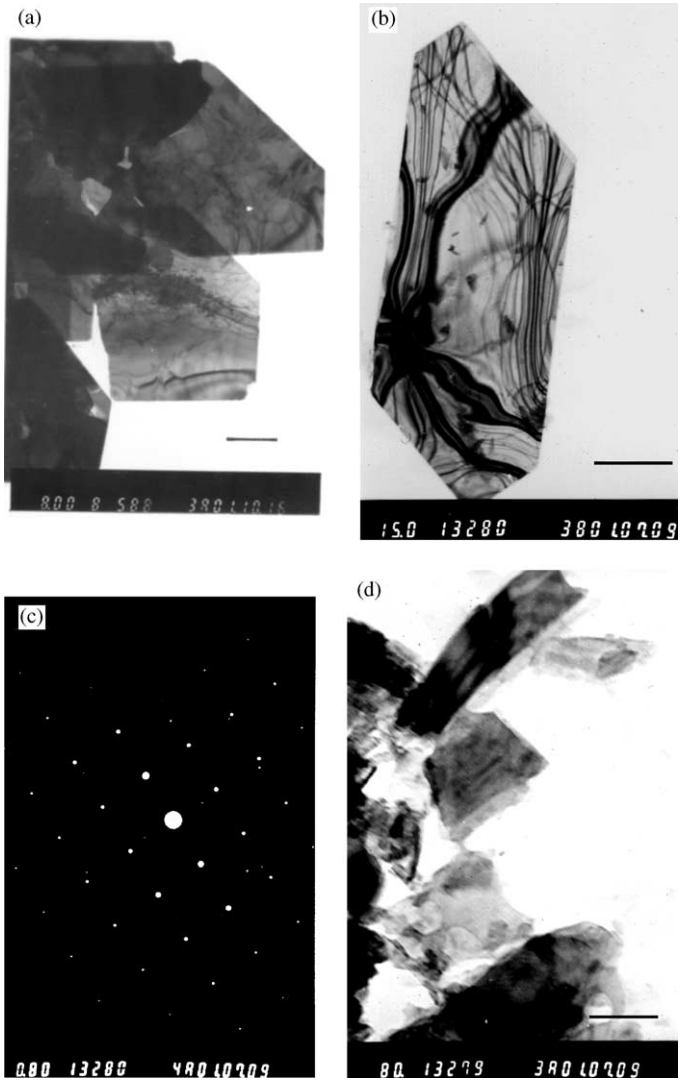

FIG. 2. (a) TEM image of SnS_2 obtained in *n*-hexane at 180–200°C for 40 h (scale bar, 1000 nm). (b) A typical hexagonal flake obtained in *n*-hexane (scale bar, 666 nm). (c) ED for the flake in Fig. 2b. (d) TEM image of SnS_2 obtained in *n*-hexane at 180–200°C for 10 h (scale bar, 125 nm).

Mössbauer spectrum of samples obtained in *n*-hexane is illustrated in Fig. 4. The corresponding isomer shift (δ) is 1.002 mm s^{-1} for the products, which is consistent with the Sn^{IV} oxidation state. The absorption (peak) position shows the characteristic absorption of SnS_2. The full width at half-maximum (Γ) is 1.068 mm s^{-1}, which coincides with the reported value (35). In the spectrum, no absorption peak for SnS or Sn_2S_3 has been observed. The spectrum of SnS_2 obtained in cyclohexane gives similar results.

In the present process, the formation of SnS_2 is probably based on the decomposition of CS_2 and TBT. Although the precise composition of the products is not completely known in the autoclave, it could be certain that a number of decomposition reactions are possible in the process. Under

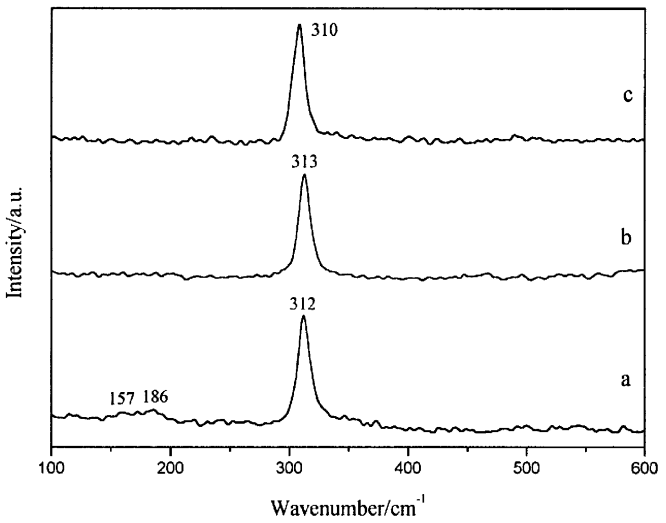

FIG. 3. Raman spectra of the samples obtained in the route: (a) in *n*-hexane with a feedstock of 1 ml:0.5 ml for TBT:CS_2, (b) in *n*-hexane with 1 ml:2 ml for TBT: CS_2, (c) in cyclohexane with 1 ml:2 ml for TBT:CS_2.

solvothermal conditions, the decomposition of CS_2 forms sulfur radicals, which attack Sn–C bonds in TBT, promoting a series of reactions. Solvothermal conditions at the same time are favorable for the decomposition of TBT between Sn and C atoms in the weak Sn-C bonds. The overall results of the process could form SnS_2. The main reactions in the process could be proposed as follows:

$$CS_2 \rightarrow S: + :CS \qquad [1]$$

$$S: + (CH_3CH_2CH_2CH_2)_4Sn \rightarrow$$

$$(CH_3CH_2CH_2CH_2)_2Sn{=}S + 2CH_3CH_2CH_2CH_2\cdot \qquad [2]$$

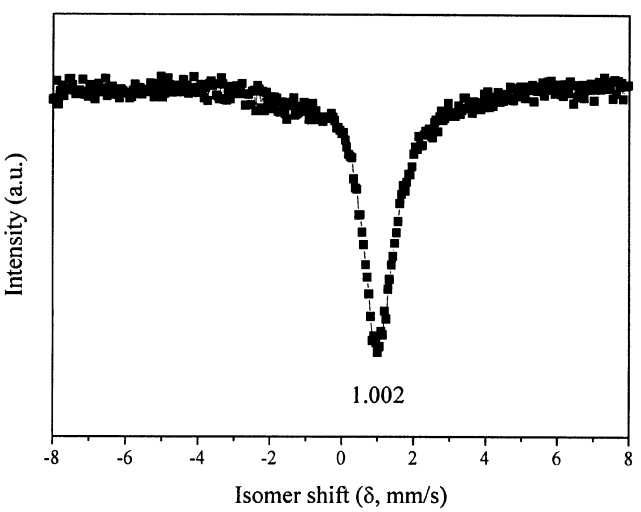

FIG. 4. Mössbauer spectrum of SnS_2 obtained in *n*-hexane.

$$S: + (CH_3CH_2CH_2CH_2)_2Sn{=}S \rightarrow$$

$$S{=}Sn{=}S + 2CH_3CH_2CH_2CH_2\cdot. \qquad [3]$$

In the reaction system, the reactions occurred in an oxygen-free state the same as in the reported routes (such as MBE (22), spray pyrolysis (23), and CVD (25–28)), so tin oxides could not form the target products. In Fig. 3a (Raman spectra), traces of SnS have been observed in SnS_2 crystallites, which indicates the feedstock of the reagents may somewhat influence the product in the route. However, the influence of the feedstock of reactants is rather inconspicuous; reaction temperature is the main factor. When the temperature is lower than 180°C, SnS_2 is difficult to obtain. Longer reaction time is favorable for the crystallization of SnS_2 flakes (Fig. 2). In the crystallization process, the formation of the flakelike nanocrystalline SnS_2 is mainly caused by the intrinsic anisotropic nature of SnS_2 because SnS_2 has a CdI_2-related crystal structure (36). It consists of two layers of hexagonal closed-packed sulfur anions with sandwiched tin cations, which are octahedrally coordinated by six nearest-neighbor sulfur atoms. Each sulfur atom is nested at the top of a triangle of Sn atoms. Adjacent S–Sn–S layers are bound by weak van der Waals interactions in the crystals. In the route, the flakelike morphologies of the SnS_2 crystallites have not been obviously affected by reagents.

4. CONCLUSIONS

SnS_2 nanoflakes with hexagonal phase structure have been synthesized from reactions between an organotin precursor tetrabutyltin and carbon disulfide under solvothermal conditions at 180–200°C in hexane solutions. The formation of SnS_2 was proposed from the decomposition of reactants and the attack of sulfur radicals. The reaction temperature played an important role in the formation of the nanoflakes. The flakelike morphologies of the as-prepared SnS_2 crystals are mainly caused by the intrinsic anisotropy of SnS_2. This available and useful method has been employed to deposit the SnS_2 films on the different substrates.

ACKNOWLEDGEMENTS

Financial support of this work by the National Natural Science Foundation of China and the 973 Projects of China is gratefully acknowledged. The authors thank Prof. Jian Zuo, Cunyi Xu, Mingrong Ji, Dr. Xiaoming Liu, and Wanqun Zhang for their help with equipment facilities.

REFERENCES

1. R. Suryanarayanan, *Phys. Status Solidi B* **85,** 9 (1978).
2. M. G. Bawendi, M. L. Steigerwald, and L. E. Brus, *Annu. Rev. Phys. Chem.* **41,** 477 (1990).
3. N. Peyghambarian, B. Fluegel, D. Hulin, A. Migus, M. Joffre, A. Antonetti, S. W. Koch, and M. Lindberg, *IEEE J. Quantum Electron.* **25,** 2516 (1989).
4. A. Agarwal, P. D. Patel, and D. Lakshminarayana, *J. Crystal Growth* **142,** 344 (1994).
5. C. D. Lokhande, *J. Phys. D*: *Appl. Phys.* **23,** 703 (1990).
6. (a) J. J. Loferski, *J. Appl. Phys.* **27,** 777 (1956); (b) G. Domingo, R. S. Itoga, and C. R. Cannewurf, *Phys. Rev.* **143,** 536 (1966).
7. D. Chu, R. M. Walser, R. W. Bene, and T. H. Courtney, *Appl. Phys. Lett.* **24,** 479 (1974).
8. S. G. Patil and R. H. Fredgold, *J. Pure Appl. Phys.* **4,** 718 (1971).
9. D. L. Greenway and R. Nitsche, *J. Phys. Chem. Solids* **26,** 1445 (1965).
10. C. R. Whitehouse and A. A. Balchin, *J. Mater. Sci.* **144,** 2516 (1979).
11. R. Nitsche, *J. Phys. Chem. Solids* **17,** 163 (1960).
12. (a) H. Martinez, C. Auriel, M. Loudet, and G. Pfister-Guillouzo, *Appl. Surf. Sci.* **103,** 149 (1996); (b) G. A. Shaw and I. P. Parkin, *Main Group Met. Chem.* **19,** 499 (1996).
13. R. Coustal, *J. Chim. Phys.* **31,** 277 (1931).
14. R. W. Parry, "Inorganic Synthesis," Vol. 12. Mc Graw-Hill, New York, 1995.
15. I. P. Parkin and A. T. Rowley, *Polyhedron* **12,** 2961 (1993).
16. P. Balaz, T. Ohtani, Z. Bastl, and E. Boldizarova, *J. Solid State Chem.* **144,** 1 (1999).
17. S. R. Bahr, P. Boudjouk, and G. J. McCarthey, *Chem. Mater.* **4,** 383 (1992).
18. P. Boudjouk, D. J. Seidler, D. Grier, and G. J. McCarthey, *Chem. Mater.* **8,** 1189 (1996).
19. T. Shibata, T. Miura, T. Kishi, and T. Nagai, *J. Crystal Growth* **106,** 593 (1990).
20. J. George and C. K. Valsala Kumari, *J. Crystal Growth* **63,** 233 (1983).
21. G. Scamarsio, A. Cingolani, and M. Sibilano, *Solid State Commun.* **72,** 1039 (1989).
22. K. W. Nnebesny, G. E. Collins, P. A. Lee, L. K. Chau, J. Danziger, E. Osburn, and N. R. Armstrong, *Chem. Mater.* **3,** 829 (1991).
23. A. Ortiz and S. Lopez, *J. Semicond. Sci. Technol.* **9,** 2130 (1994).
24. B. R. Sankapal, R. S. Mane, and C. D. Lokhande, *Mater. Res. Bull.* **35,** 2027 (2000).
25. A. Ortiz, J. C. Alonso, M. Garcia, and J. Toriz, *J. Semicond. Sci. Technol.* **11,** 243 (1994).
26. H. M. M. I. Simpson, *J. Electrochem. Soc.* **122,** 444 (1975).
27. I. P. Parkin, L. S. Price, T. G. Hibbert, and K. C. Molloy, *J. Mater. Chem.* **11,** 1486 (2001).
28. L. S. Price, I. P. Parkin, A. M. E. Hardy, R. J. H. Clark, T. G. Hibbert, and K. C. Molloy, *Chem. Mater.* **11,** 1792 (1999).
29. B. Hai, K. B. Tang, C. R. Wang, C. H. An, Q. Yang, G. Z. Shen, and Y. T. Qian, *J. Crystal Growth* **225,** 92 (2001).
30. (a) J. P. Espinós, A. R. González-Elipe, L. Hernán, J. Morales, L. Sánchez, and J. Santos, *Surf. Sci.* **426,** 259 (1999); (b) C. D. Wagner, W. M. Riggs, L. E. Davis, and J. F. Moulder, *in* "Handbook of X-ray Photoelectron Spectroscope" (G. E. Muilenberg, Ed.). Perkin-Elmer Corp., Eden Prairie, MN, 1979.
31. A. W. C. Lin, N. R. Armstrong, and T. Kuwana, *Anal. Chem.* **49,** 1228 (1977).
32. C. D. Wagner, *Discuss. Faraday Soc.* **60,** 291 (1975).
33. G. Lucovsky, J. C. Mikkelsen, Jr., W. Y. Liang, R. M. White, and R. M. Martin, *Phys. Rev. B* **14,** 1663 (1976).
34. L. Abello, B. Bochu, A. Gaskov, S. Koudryavtseva, G. Lucazeau, and M. Roumyantseva, *J. Solid State Chem.* **135,** 78 (1998).
35. (a) R. H. Herber, A. E. Smelkinson, M. J. Sienko, and L. F. Schneemeyer, *J. Chem. Phys.* **68,** 3705 (1978); (b) C. P. Vicente, J. L. Tirado, P. E. Lippens, and J. C. Jumas, *Phys. Rev. B* **56,** 6371 (1997).
36. A. F. Wells, "Structural Inorganic Chemistry," 5th ed. Oxford Univ Press, London, 1984.